Journal of Alloys and Compounds 654 (2016) 392–398

Contents lists available at ScienceDirect

Journal of Alloys and Compounds

journal homepage: http://www.elsevier.com/locate/jalcom

Magnetic order and structural properties of $Tb_2Fe_2Si_2C$

R.A. Susilo [a, *], J.M. Cadogan [a], W.D. Hutchison [a], M. Avdeev [b], R. Cobas [a], S. Muñoz-Pérez [a], S.J. Campbell [a]

[a] School of Physical, Environmental and Mathematical Sciences, UNSW Canberra, Australian Defence Force Academy, Canberra, ACT 2610, Australia
[b] Bragg Institute, ANSTO, PMB 1, Menai, NSW 2234, Australia

ARTICLE INFO

Article history:
Received 20 July 2015
Received in revised form
8 September 2015
Accepted 11 September 2015
Available online 15 September 2015

Keywords:
Neutron diffraction
Mössbauer spectroscopy
Magnetic structure
Rare-earth intermetallics

ABSTRACT

The structural and magnetic properties of $Tb_2Fe_2Si_2C$ have been investigated by bulk measurements (magnetisation and specific heat), X-ray diffraction, neutron powder diffraction and ^{57}Fe Mössbauer spectroscopy over the temperature range 3 K–300 K $Tb_2Fe_2Si_2C$ is antiferromagnetic with a Néel temperature T_N of 44(2) K. The magnetic structure can be described with a propagation vector $\mathbf{k} = [0\ 0\ \frac{1}{2}]$ with the Tb magnetic moments ordering along the *b*-axis. We also observed strong magnetoelastic effects in particular along the *a*- and *c*-axes associated with the antiferromagnetic transition. The ^{57}Fe Mössbauer spectra show no evidence of magnetic splitting down to 10 K, indicating that the Fe atom is non-magnetic in $Tb_2Fe_2Si_2C$.

1. Introduction

The $R_2Fe_2Si_2C$ (R = rare-earth) series of compounds were discovered by Paccard and Paccard [1]. These quaternary compounds crystallise in the monoclinic $Dy_2Fe_2Si_2$ C-type structure with the $C2/m$ (#12) space group. An extensive range of compounds with R = Y, La–Nd, Sm, Gd–Tm and Lu has been synthesised and studied [1–3]. The R, Fe and Si atoms occupy 4*i* sites with the *m* point symmetry, generated by (*x*,0,*z*), while the C atom occupies the 2*a* site at (0,0,0) with the 2/*m* point symmetry.

These compounds are antiferromagnetic, with Néel temperatures (T_N) ranging from T_N ~ 45 K for $Tb_2Fe_2Si_2C$ to T_N ~ 2.7 K for $Tm_2Fe_2Si_2C$ [2,4]. No magnetic order was observed for $Y_2Fe_2Si_2C$, $Pr_2Fe_2Si_2C$ and $Lu_2Fe_2Si_2C$ down to 2 K. Based on magnetisation studies, the magnetism of $R_2Fe_2Si_2C$ was attributed solely to the R atoms, *i.e.* the Fe atom was reported to be non-magnetic. The magnetic structures of $Nd_2Fe_2Si_2C$ and $Tb_2Fe_2Si_2C$ were first reported by Le Roy et al. [5] who proposed a doubled antiferromagnetic structure along the *c*-axis ($\mathbf{k} = [0\ 0\ \frac{1}{2}]$) with both the R and Fe sublattices being magnetically ordered, almost perpendicular to each other. Recently, we used neutron diffraction on $Gd_2Fe_2Si_2C$ and $Ho_2Fe_2Si_2C$ to show that the Gd and Ho sublattices order antiferromagnetically along the *b*-axis with a propagation vector $\mathbf{k} = [0\ 0\ \frac{1}{2}]$ and on the basis of ^{57}Fe Mössbauer spectroscopy we found that the Fe atom carries no magnetic moment in these compounds [6,7].

In this paper, we present the results of our re-examination of the magnetic and structural properties of $Tb_2Fe_2Si_2C$ using x-ray diffraction, magnetisation, specific heat measurements, neutron powder diffraction and ^{57}Fe Mössbauer spectroscopy. Our main interest arises from the inconsistent results between magnetic studies which suggest that the Fe atom is non-magnetic [4] and the neutron diffraction study of Le Roy et al. [5] who proposed magnetic order in both the Tb and Fe sublattices. Our findings reveal that while our neutron diffraction refinements cannot definitively confirm or rule out the existence of magnetic order of the Fe sublattice, no magnetic splitting is observed in the ^{57}Fe Mössbauer spectra collected below T_N, thus establishing the absence of magnetic ordering of the Fe sublattice in this compound. In addition, our low temperature x-ray diffraction measurements show large magnetoelastic effects with a magnitude of ~5×10^{-3} (at 20 K) associated with the antiferromagnetic transition below $T_N = 44(2)$ K, with the effects being prominent along the *a* and *c* directions.

2. Experimental methods

The $Tb_2Fe_2Si_2C$ samples were prepared by arc-melting the high purity elements (at least 99.9 wt%) under an argon atmosphere. The

* Corresponding author.
E-mail address: resta.susilo@student.adfa.edu.au (R.A. Susilo).

http://dx.doi.org/10.1016/j.jallcom.2015.09.092
0925-8388/

ingots were turned and re-melted several times to ensure homogeneity. X-ray powder diffraction (XRD) patterns were collected at various temperatures between 300 K and 20 K using a PANalytical Empyrean diffractometer (Cu-K_α radiation) equipped with an Oxford Instruments Phenix closed-cycle refrigerator.

Magnetisation and zero field specific heat data were measured using a Quantum Design Physical Property Measurement System (PPMS). Magnetisation data were collected in the temperature range between 2 K and 300 K in an applied field $\mu_0 H = 1$ T, while the specific heat measurement was performed using a relaxation method between 2 K and 300 K. The ordering temperature was determined from the peak of the temperature derivatives of magnetisation and specific heat data.

Neutron diffraction experiments were carried out on the Echidna high resolution powder diffractometer [8] at the OPAL reactor in Sydney, Australia with an incident neutron wavelength of 2.4395(5) Å. Short duration neutron diffraction patterns were collected at various temperatures between 3 K and 60 K to provide overall insight into the structural and magnetic behaviour over this temperature range. Long duration patterns were obtained at 3 K and 60 K – below and above the antiferromagnetic transition T_N = 44(2) K – for more detailed investigations. All diffraction patterns were corrected for absorption effects and were refined by the Rietveld method using the FullProf/Winplotr software [9,10].

^{57}Fe Mössbauer spectra were collected in standard transmission mode using a ^{57}Co–Rh source. The spectrometer was calibrated with an α-Fe foil at room temperature and the sample temperature was varied from 10 K to 80 K using a vibration-isolated, closed-cycle refrigerator. All spectra were fitted using the Recoil software [11].

3. Results

3.1. Crystal structure

Refinement of the X-ray diffraction pattern collected at room temperature confirmed the formation of the monoclinic $Dy_2Fe_2Si_2C$-type structure with impurity phases (identified as $TbC_{0.33}$ (terbium carbide) and unreacted silicon) present in the total amount of ~3 wt%. The refined pattern is shown in Fig. 1. The lattice parameters of $Tb_2Fe_2Si_2C$ obtained from this refinement are a = 10.628(1) Å, b = 3.9362(4) Å, c = 6.7701(6) Å and β = 129.32(1)°, in good agreement with the values reported by Paccard and Paccard [1].

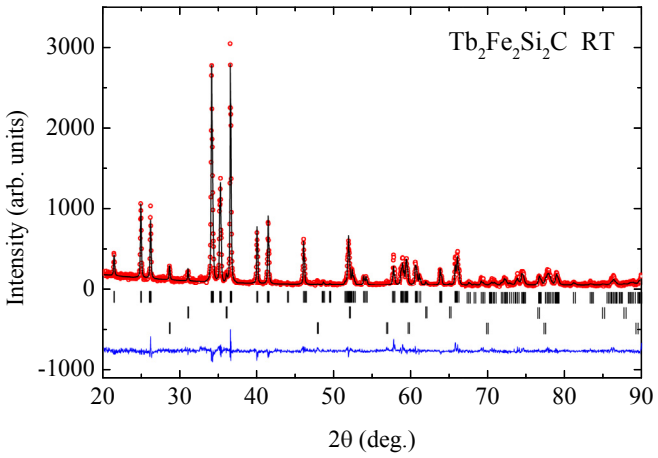

Fig. 1. Rietveld refinement of the X-ray diffraction pattern of $Tb_2Fe_2Si_2C$ collected at room temperature (Cu-K_α radiation). The Bragg markers from top to bottom represent $Tb_2Fe_2Si_2C$, $TbC_{0.33}$ and Si, respectively.

3.2. Magnetic properties

In Fig. 2, we present the dc (molar) magnetic susceptibility of $Tb_2Fe_2Si_2C$ obtained with an applied field of $\mu_0 H = 1$ T. The antiferromagnetic transition at T_N = 44 K is indicated by a cusp-like transition in the susceptibility data. This result is in excellent agreement with the previously reported ordering temperature of 45 K [4]. The Curie–Weiss fit to the inverse molar susceptibility (inset in Fig. 2), yields a paramagnetic Curie temperature of θ_P = +36(2) K and an effective magnetic moment of μ_{eff} = 9.76(4) μ_B, which agrees well with the theoretical μ_{eff} of 9.72 μ_B expected for the Tb^{3+} ion. Further, this result suggests that the Fe atom is non-magnetic in $Tb_2Fe_2Si_2C$.

In Fig. 3, we show the low temperature specific heat data, C_P, of $Tb_2Fe_2Si_2C$. It is clear that the specific heat shows a λ-type anomaly at 44 K which is consistent with the antiferromagnetic transition seen in the dc susceptibility at 44 K. From the C_P data, we can also calculate the magnetic contribution to the entropy, S_{mag}, of $Tb_2Fe_2Si_2C$ by integrating C_{mag}/T, where C_{mag} is the magnetic contribution to the specific heat. To this end, we used the specific heat of $Y_2Fe_2Si_2C$ as a non-magnetic background. The non-magnetic contribution is then removed, taking into account the molar mass difference between $Y_2Fe_2Si_2C$ and $Tb_2Fe_2Si_2C$, following the 'many-Debye' method of Bouvier et al. [12]. The normalised (mass corrected) C_P data for $Y_2Fe_2Si_2C$ are also shown in Fig. 3. The calculated values of the magnetic entropy of $Tb_2Fe_2Si_2C$ are shown in the inset of Fig. 3. The magnetic entropy released at T_N is 10.7 J mol^{-1} K^{-1} which is close to $R\ln(4)$ = 11.53 J mol^{-1} K^{-1} which suggests that the magnetic ground state consists of four levels.

3.3. Low temperature X-ray diffraction

In Fig. 4, we show the temperature dependence of the lattice parameters and the unit cell volume of $Tb_2Fe_2Si_2C$. This compound does not undergo a structural phase transition down to the lowest measurement temperature of 20 K. The lattice parameters and the unit cell volume decrease monotonically as the temperature is decreased to T_N ~ 45 K, however anomalies are observed upon cooling below the Néel temperature. The *ac*-plane of the unit cell

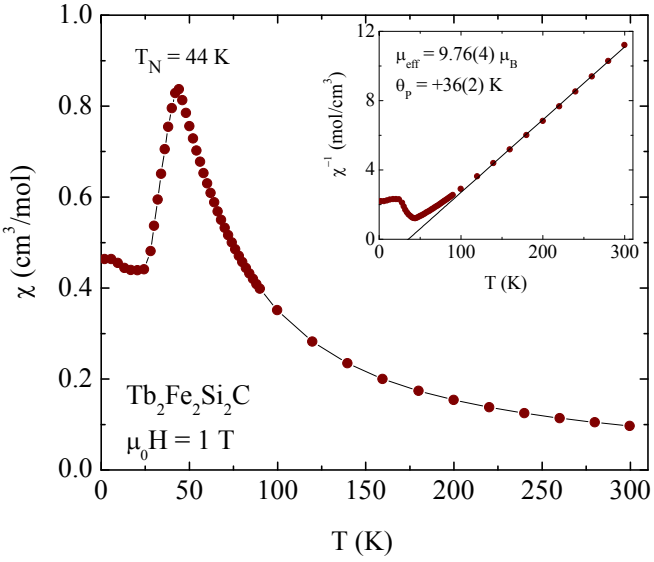

Fig. 2. DC susceptibility of $Tb_2Fe_2Si_2C$ obtained in field-cooled (FC) mode with an applied field of $\mu_0 H$ = 1 T. The inset shows the inverse susceptibility and a fit to the Curie–Weiss law.

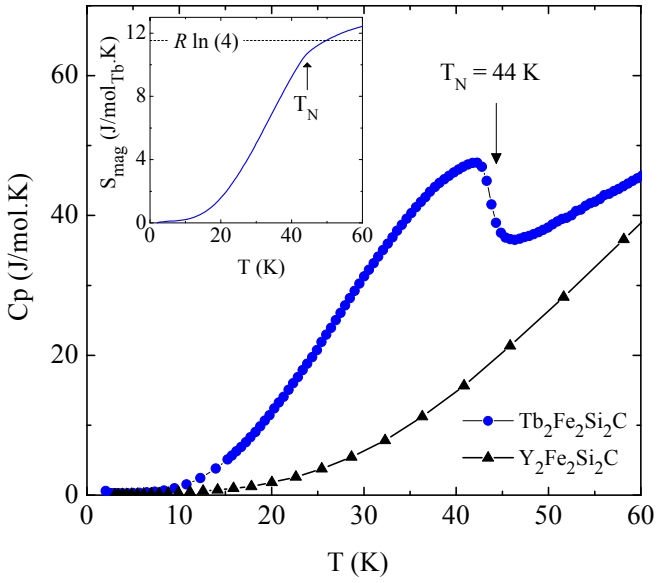

Fig. 3. Zero field specific heat of $Tb_2Fe_2Si_2C$ and the normalised specific heat of $Y_2Fe_2Si_2C$. The inset shows the calculated magnetic entropy for $Tb_2Fe_2Si_2C$.

expands anomalously, as indicated by the increase in the *a*, *c* and β parameters as the temperature is lowered. Interestingly, this lattice expansion is compensated by an anomalous lattice contraction in the *b* direction, resulting in the small net expansion of the unit cell volume. A similar behaviour in the lattice parameters was observed previously in TbFeSi [13,14]. We note that the anomaly in the lattice *b* parameter is already seen below ~100 K, far above the Néel temperature.

In order to better understand these lattice anomalies, we estimated the non-magnetic background by fitting the lattice parameters and the unit cell volume data above T = 70 K (paramagnetic state) with a second-order polynomial (see e.g. Ref. [15]). The fitted curves were then extrapolated to T = 0 K and are plotted as solid lines in Fig. 4. The *b* parameter already deviates from the estimated non-magnetic background below ~100 K, which implies that there is an additional contribution to the lattice parameter beside the phonon contribution. It is possible that this anomalous behaviour in the paramagnetic region is due to crystal field effects as observed in the RSb [16] and RCu_2 [17] systems. The differences between the experimental data and the fitted curves were used to estimate the change in lattice parameters due to the presence of exchange striction. Since the anomaly is quite pronounced along the *a*- and *c*-axes, we focus our analyses on the changes in the *a*-axis and *c*-axis (Δa and Δc) with temperature as shown in Fig. 5.

It is known that the lattice change due to exchange striction is proportional to the ordered moment (e.g. Refs. [18,19]). Assuming that the magnetic moment and the reduced magnetisation (and hence, the Brillouin function) follow the same temperature dependence, it is expected that the lattice change due to exchange striction will follow a Brillouin function. As can be seen in Fig. 5, the temperature dependence of Δa and Δc for $Tb_2Fe_2Si_2C$ below 45 K can be fitted reasonably well with a Brillouin function for Tb^{3+} ($J = 6$), indicating the dominant contribution from the exchange interaction between the Tb atoms. The least squares fitting of the lattice changes to the Brillouin function in Fig. 5 yield $T_N = 44(2)$ K and $T_N = 42(2)$ K using the *a*- and *c*-axes, respectively.

It is also interesting to note the observation of a large spontaneous magnetostriction along the *a*- and *c*-axes with a magnitude of ~5×10^{-3} Å at 20 K (Fig. 5). This value is comparable to the spontaneous magnetostriction of other R-Fe-based compounds such as Tb_2Fe_{17} [20], $TbFe_{11}Ti$ [21] and $Tb_2Fe_{14}B$ [22], although unlike those compounds, we observed only small magnetovolume effects in $Tb_2Fe_2Si_2C$.

3.4. Neutron diffraction

In Fig. 6, we show the set of neutron diffraction patterns of $Tb_2Fe_2Si_2C$ collected at various temperatures between 3 K and 60 K over the angular range $8° \leq 2\theta \leq 50°$. Several additional magnetic peaks are seen in the diffraction patterns collected below 45 K, with the strongest magnetic peak occurring at $2\theta \sim 14°$ and indexed as $\left(00\frac{1}{2}\right)$. Tracking the temperature dependence of the intensity of this magnetic peak allows us to determine the ordering temperature of $Tb_2Fe_2Si_2C$ to be ~45 K (inset of Fig. 6), fully consistent with

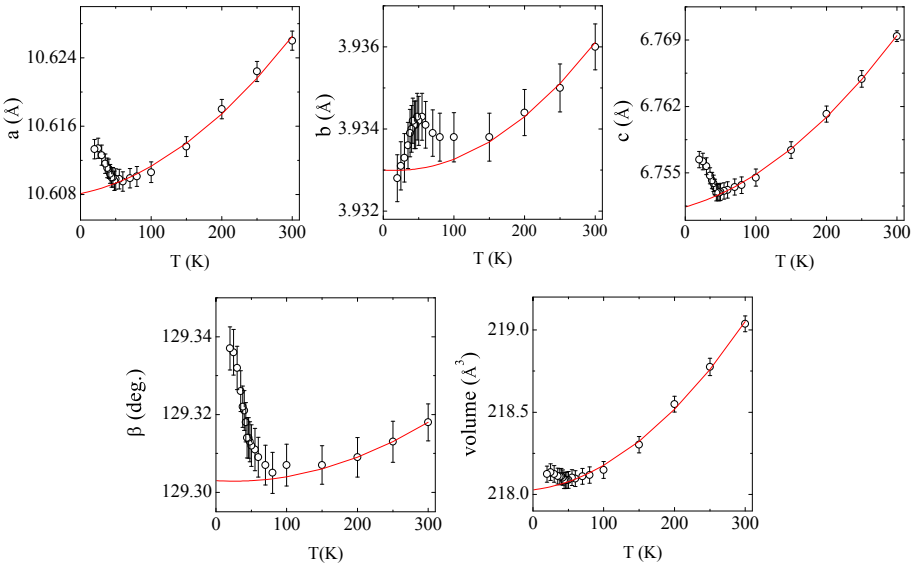

Fig. 4. Temperature dependence of the lattice parameters and the unit cell volume of $Tb_2Fe_2Si_2C$. The solid line represents a fit to the experimental data using a second-order polynomial as discussed in the text.

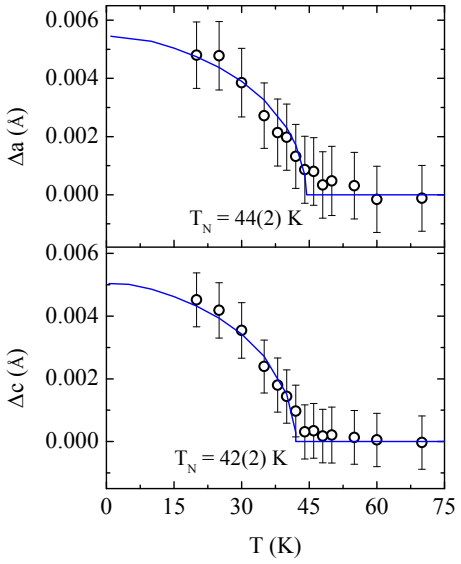

Fig. 5. Temperature dependence of Δa and Δc, the changes in the a and c lattice parameters, as described in the text. The solid lines represent fits with a $J = 6$ Brillouin function.

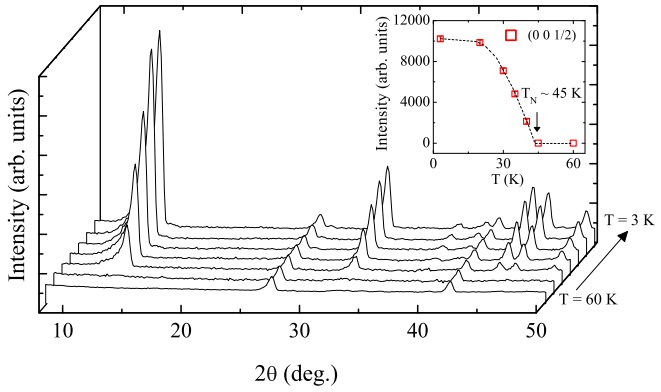

Fig. 6. Neutron powder diffraction patterns of $Tb_2Fe_2Si_2C$ obtained at 60 K, 45 K, 40 K, 35 K, 30 K, 20 K and 3 K (bottom to top; neutron wavelength $\lambda = 2.4395(5)$ Å). The inset shows the temperature dependence of the $\left(00\frac{1}{2}\right)$ magnetic peak with the dashed line acting as a guide to the eye.

the results from magnetisation (Fig. 2) and specific heat (Fig. 3) measurements.

Neutron diffraction patterns collected above and below the Néel temperature are shown in Fig. 7. As expected, refinement of the 60 K pattern of $Tb_2Fe_2Si_2C$ above T_N shows only nuclear scattering from the monoclinic $C2/m$ space group, with the parameters derived from the refinement summarised in Table 1.

The neutron diffraction pattern at 3 K presents several additional magnetic peaks arising from the Tb sublattice which can be indexed with a propagation vector $\mathbf{k} = [0\ 0\ \frac{1}{2}]$, *i.e.* cell-doubling along the c-axis. In order to determine the symmetry-allowed magnetic structures for the Tb atom at the 4*i* site, we carried out representational analysis using the BASIREPS program, part of FullProf suite [9]. The decomposition of the magnetic representation comprises four one-dimensional representations:

$$\Gamma^{4i} = 1\Gamma_1 + 2\Gamma_2 + 2\Gamma_3 + \Gamma_4. \quad (1)$$

The basis vectors of these irreducible representations are given in Table 2.

From Table 2, it can be seen that there are two symmetry-

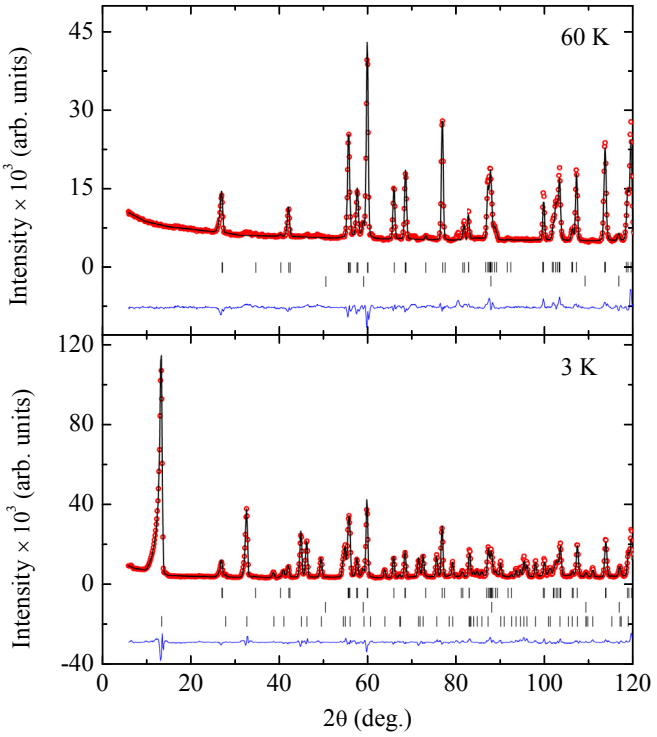

Fig. 7. Rietveld refinement of the neutron diffraction patterns of $Tb_2Fe_2Si_2C$ collected at 60 K (top) and 3 K (bottom) with a neutron wavelength $\lambda = 2.4395(5)$ Å. The rows of Bragg markers represent $Tb_2Fe_2Si_2C$ (nuclear), $TbC_{0.33}$ and $Tb_2Fe_2Si_2C$ (magnetic) from top to bottom, respectively.

Table 1
Crystallographic and magnetic parameters of $Tb_2Fe_2Si_2C$ derived from the refinement of the neutron diffraction patterns obtained at 3 K and 60 K.

	60 K	3 K
x_{Tb}	0.5612(12)	0.5613(8)
z_{Tb}	0.295(2)	0.293(1)
x_{Fe}	0.203(1)	0.201(2)
z_{Fe}	0.097(2)	0.095(2)
x_{Si}	0.158(2)	0.161(3)
z_{Si}	0.714(3)	0.714(4)
a (Å)	10.6064(4)	10.6106(5)
b (Å)	3.9330(2)	3.9322(2)
c (Å)	6.7515(4)	6.7559(3)
β (°)	129.30(1)	129.33(1)
μ_{Tb} (μ_B)	–	8.0(1)
R_p(%); R_{wp}(%)	15.2; 13.0	11.1; 11.5
R_{Bragg}(%); R_F(%)	10.2; 7.2	6.5; 4.6
R_{mag}(%)	–	6.1

allowed orientations of the Tb magnetic moments; in the ac-plane and along the b-axis. The 3 K neutron pattern can be well fitted with the Tb magnetic moments aligned along the b-axis corresponding to the Γ_4 representation which is equivalent to the C_{2c} $2/m$ magnetic space group (#12.6.71 based on Litvin's scheme

Table 2
Representational analysis for the Tb atom at the 4*i* site in $Tb_2Fe_2Si_2C$ with a propagation vector $\mathbf{k} = [0\ 0\ \frac{1}{2}]$.

	Tb_1 (x,0,z)	Tb_2 ($-x$,0,$-z$)
Γ_1	M_y	M_y
Γ_2	M_x,M_z	$-M_x$,$-M_z$
Γ_3	M_x,M_z	M_x,M_z
Γ_4	M_y	$-M_y$

[23]). The refinement parameters for the 3 K pattern are given in Table 1.

The magnetic structure of $Tb_2Fe_2Si_2C$ consists of antiferromagnetic ordering of the Tb magnetic moments along the *b*-axis as shown in Fig. 8. The dominant ferromagnetic coupling between the Tb magnetic moments within a unit cell is reflected in the positive paramagnetic Curie temperature obtained from susceptibility measurements (Section 3.2). The refined Tb moment at 3 K is 8.0(1) μ_B, 11% smaller than the 'free-ion' value of 9 μ_B. The reduction of the Tb moment is most likely the result of strong crystal field effects, as commonly observed in rare-earth intermetallic compounds.

Our refined magnetic structure is slightly different from the magnetic structure reported by Le Roy et al. [5] in which the Tb moment is canted away from the *b*-axis towards an intermediate planar arrangement. In order to check for the possibility of a canted magnetic structure at low temperature, we carried out refinements to the 3 K neutron pattern by varying the *x*- and *z*-components of the Tb magnetic moments, *i.e.* mixing the Γ_2 and Γ_4 representations. However, this approach did not improve the quality of the refinement; this finding suggests that a single irreducible representation (Γ_4) is sufficient to describe the magnetic structure, consistent with the Landau theory of second-order phase transitions [24].

The neutron diffraction pattern obtained at 1.2 K by Le Roy et al. shows weak incommensurate magnetic peaks at $2\theta_1 \sim 12^\circ$ and $2\theta_2 \sim 27^\circ$ ($d_1 = 11.89$ Å and $d_2 = 5.26$ Å) [5], while the refinement to our 3 K neutron diffraction pattern (Fig. 7) shows no unfitted magnetic peaks. This indicates that the incommensurate magnetic peaks observed in the previous study [5] are most likely magnetic peaks from an impurity phase and cannot be attributed to a change in the magnetic structure from collinear antiferromagnetic to incommensurate. To this end, we systematically carried out simulations in an attempt to identify the possible impurity phase with the incommensurate magnetic structure. We found that the magnetic peaks observed previously [5] can be reproduced by considering the incommensurate magnetic structure of $TbFe_2Si_2$ ($\mathbf{k} = [0, 0.3225, 0.1778]$) [25] which orders antiferromagnetically below 7 K [25–27].

In Fig. 9, we show the temperature dependence of the lattice parameters and the Tb moment obtained from the refinement of the neutron diffraction patterns. The temperature dependence of the refined Tb moment can be fitted with a $J = 6$ Brillouin function with $T_N = 44.2(2)$ K. We again found unusual behaviour of the lattice parameters below T_N with the *a*- and *c*-parameters increasing while the *b*-parameter decreases upon cooling, as observed in the low temperature x-ray diffraction measurements (*cf.* Fig. 4).

It should be noted that several attempts were made to refine the pattern at 3 K by considering both the magnetic ordering of the Tb and Fe sublattices for all possible irreducible representations

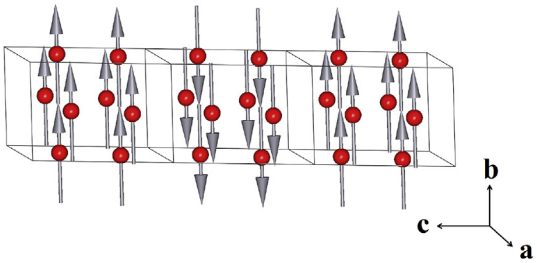

Fig. 8. The magnetic structure of $Tb_2Fe_2Si_2C$ at 3 K. Each block corresponds to a nuclear unit cell. The Fe, Si and C atoms are excluded for clarity.

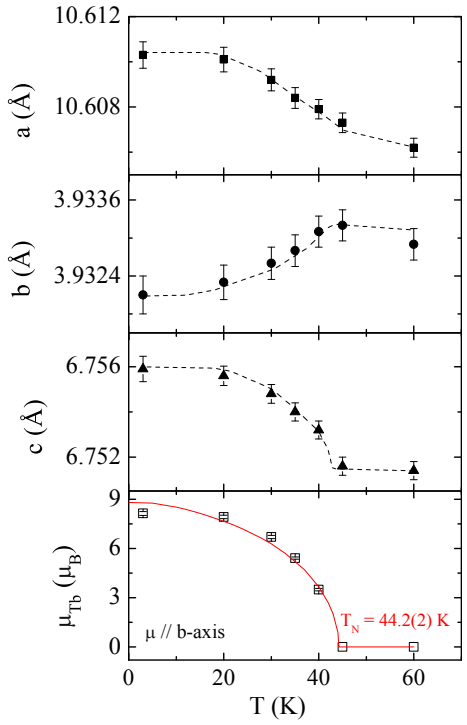

Fig. 9. Temperature dependence of the lattice parameters and the Tb moment of $Tb_2Fe_2Si_2C$ derived from the refinement of the neutron diffraction patterns. The solid line represents a fit to the $J = 6$ Brillouin function with the dashed lines acting as guides to the eye.

shown in Table 2. In all attempts, we found the refined Fe moment to be in the range of 1.0 − 1.5 μ_B. However, the results are virtually indistinguishable *i.e.* the refinements yield the same R-factors as in the refinement without the Fe moment. Based on this result, we concluded that neutron powder diffraction alone is insufficient to give a clear, unambiguous description of the magnetism of $Tb_2Fe_2Si_2C$, in particular regarding the behaviour of the Fe sublattice. Therefore, we turned to ^{57}Fe Mössbauer spectroscopy which is a direct probe of the Fe site.

3.5. ^{57}Fe Mössbauer spectroscopy

^{57}Fe Mössbauer spectra of $Tb_2Fe_2Si_2C$ collected well above T_N (at 80 K) and below T_N (at 10 K) are shown in Fig. 10. The 80 K spectrum can be fitted using one doublet with a quadrupole splitting of QS = 0.630(4) mm/s and an isomer shift of IS = 0.095(2) mm/s relative to α-Fe at room temperature. The 10 K spectrum (well below $T_N = 44(2)$ K) shows no magnetic splitting which gives unequivocal evidence that the Fe atom is non magnetic in this compound. A small line broadening and an asymmetric doublet are seen in the 10 K spectrum which reflects the presence of a small transferred hyperfine field. The temperature dependences of the ^{57}Fe hyperfine parameters obtained at various temperatures between 10 K and 80 K are shown in Fig. 11.

Similar to the case of $Ho_2Fe_2Si_2C$ [7], a small line broadening is observed on cooling below $T_{onset} = 46$ K, with the broadening considered to be due to the transferred hyperfine field from the surrounding Tb moments. The quadrupole splitting also shows an increase below T_N, reaching a maximum value of QS = 0.643(4) mm/s at 35 K. This behaviour may reflect the presence of a small transferred hyperfine field at the ^{57}Fe nucleus due to the ordering of the Tb sublattice. It is also possible that the anomalous behaviour in the lattice parameters (Section 3.3)

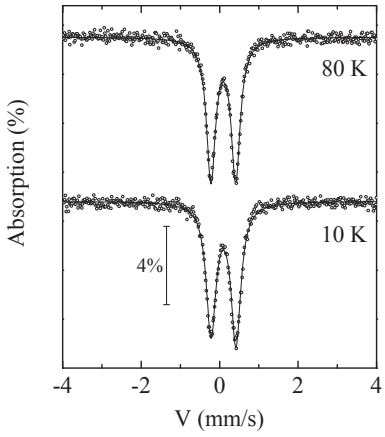

Fig. 10. ^{57}Fe Mössbauer spectra of $Tb_2Fe_2Si_2C$ collected at 80 K and 10 K.

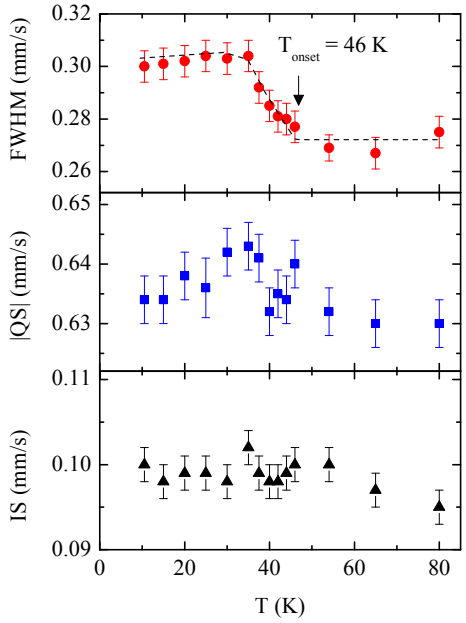

Fig. 11. Temperature dependence of the hyperfine parameters of $Tb_2Fe_2Si_2C$. The dashed line is a guide to the eye. FWHM, QS and IS represent the linewidth, quadrupole splitting and isomer shift, respectively.

contributes to the change in quadrupole splitting values. The isomer shift values are found to remain constant at low temperature below T ~ 50 K but decrease steadily above 50 K, consistent with the behaviour expected from the second-order Doppler shift.

4. Discussion

Neutron diffraction patterns of $Tb_2Fe_2Si_2C$ collected below T_N = 44(2) K confirm the antiferromagnetic ordering of the Tb sublattice along the *b*-axis with a propagation vector of $\mathbf{k} = [0\ 0\ \frac{1}{2}]$. This magnetic structure is similar to those observed in $Gd_2Fe_2Si_2C$ [6] and $Ho_2Fe_2Si_2C$ [7]. We note that refinement of the neutron powder diffraction data alone is insufficient to answer the question of whether or not the Fe is magnetic in $Tb_2Fe_2Si_2C$. Given the identical point symmetries of the Tb and Fe atoms in the *C*2/*m* space group (both occupy 4*i* sites), it is impossible to distinguish the magnetic contribution from both the Tb and Fe sublattices if they order simultaneously below T_N with the same propagation vector $\mathbf{k} = [0\ 0\ \frac{1}{2}]$. However, the use of ^{57}Fe Mössbauer spectroscopy as a direct probe at the Fe site gives strong evidence that the Fe atom is in fact non-magnetic in $Tb_2Fe_2Si_2C$, supporting the results from the Curie–Weiss fit (Section 3.2) which suggests that there is no contribution due to the Fe sublattice ordering. A small line broadening below T_N is associated with the presence of a transferred hyperfine field from the ordering of the Tb sublattice and we estimate this transferred hyperfine field to be around 0.4 T at 10 K. By comparison, if the Fe atom were to carry a significant magnetic moment such as ~1.7 μ_B as derived from the previous neutron diffraction studies [5] or 1.5 μ_B as obtained from our neutron diffraction refinements (Section 3.4), one would expect a hyperfine field of at least 10 T at the ^{57}Fe nucleus.

Low temperature X-ray diffraction and neutron diffraction measurements show unusual behaviour in the lattice parameters on cooling below T_N which is associated with the spontaneous magnetostriction due to the antiferromagnetic ordering of the Tb sublattice. Comparison of the temperature dependence of the lattice parameters and the Tb moment as in Fig. 9, reveals that the lattice shrinks along the direction of the Tb moment, and expands perpendicular to the moment direction. In order to understand the relationship between the lattice anomalies and the direction of the Tb magnetic moment, we have checked the secondary structural parameters, *i.e.* the temperature dependence of the interatomic distances between Tb atoms and the atomic displacement of the Tb atom. However, our examination of these structural parameters does not reveal any systematic trends, due to the large uncertainties in the data. Further studies such as more extensive high-resolution synchrotron radiation studies would clarify this behaviour.

5. Conclusion

Neutron diffraction studies have established that the magnetic order of the Tb sublattice in $Tb_2Fe_2Si_2C$ is commensurate antiferromagnetic along the *b*-axis with a propagation vector $\mathbf{k} = [0\ 0\ \frac{1}{2}]$ below T_N = 44(2) K. On the basis of ^{57}Fe Mössbauer spectroscopy, we find no evidence of magnetic splitting below T_N thus establishing the absence of magnetic ordering of the Fe sublattice. A slight line broadening observed in the spectra taken below the antiferromagnetic transition reflects the presence of a transferred hyperfine field of order 0.4 T at 10 K from the ordering of the Tb sublattice.

Acknowledgements

RAS acknowledges receipt of a University International Postgraduate Award (UIPA) from the University of New South Wales. The authors would like to thank the reviewers for their comments and suggestions which improved the quality of the paper.

References

[1] L. Paccard, D. Paccard, J. Less Comm. Met. 136 (1988) 297–301.
[2] R. Pöttgen, T. Ebel, C.B.H. Evers, W. Jeitschko, J. Sol. State Chem. 114 (1995) 66–72.
[3] T. Hüfken, A.M. Witte, W. Jeitschko, J. Alloys Compd. 266 (1998) 158–163.
[4] D. Schmitt, D. Paccard, L. Paccard, Solid State Commun. 84 (1992) 357–361.
[5] J. Le Roy, D. Paccard, C. Bertrand, J.L. Soubeyroux, J. Bouillot, L. Paccard, D. Schmitt, Solid State Commun. 86 (1993) 675–678.
[6] D.H. Ryan, N. Mas, R.A. Susilo, J.M. Cadogan, R. Flacau, J. Phys. Condens. Matter 27 (2015) 146005.
[7] R.A. Susilo, J.M. Cadogan, R. Cobas, W.D. Hutchison, M. Avdeev, S.J. Campbell, J. Appl. Phys. 117 (2015), 17C113.
[8] K.-D. Liss, B. Hunter, M. Hagen, T. Noakes, S. Kennedy, Phys. B 385–386 (2006) 1010–1012.
[9] J. Rodríguez-Carvajal, Phys. B 192 (1993) 55–69.
[10] T. Roisnel, J. Rodríguez-Carvajal, Mat. Sci. Forum 378–381 (2001) 118–123.

[11] K. Lagarec, D.G. Rancourt, Recoil-mössbauer Spectral Analysis Software for Windows, Ver. 1.0, Department of Physics, University of Ottawa, Ottawa, ON, Canada, 1998.
[12] M. Bouvier, P. Lethuillier, D. Schmitt, Phys. Rev. B 43 (1991) 13137–13144.
[13] R. Welter, G. Venturini, B. Malaman, J. Alloys Compd. 189 (1992) 49–58.
[14] R. Welter, PhD thesis, Université Henri Poincaré - Nancy I, France, 1994.
[15] Y. Fei, in: T. Ahren (Ed.), Mineral physics and Crystallography: a Handbook of Physical Constants, Vol. 2, American Geophysical Union, 1995.
[16] M.E. Mullen, B. Lüthi, P.S. Wang, E. Bucher, L.D. Longinotti, J.P. Maita, H.R. Ott, Phys. Rev. B 10 (1974) 186–199.
[17] E. Gratz, M. Rotter, A. Lindbaum, H. Muller, E. Bauer, H. Kirchmayer, J. Phys. Condens. Matter 5 (1993) 567.
[18] F.J. Darnell, Phys. Rev. 130 (1963a) 1825–1828.
[19] F.J. Darnell, Phys. Rev. 132 (1963b) 1098–1100.
[20] A. Andreev, F. de Boer, T. Jacobs, K. Buschow, Phys. B 175 (1991) 361–369.
[21] A.V. Andreev, S.M. Zadvorkin, Philos. Mag. B 77 (1998) 147–161.
[22] N. Yang, K. Dennis, R. McCallum, M. Kramer, Y. Zhang, P. Lee, J. Magn. Magn. Mater. 295 (2005) 65–76.
[23] D.B. Litvin, Acta Crystallogr. Sect. A 64 (2008) 419–424.
[24] L.D. Landau, E.M. Lifshitz, Statistical Physics, Course of Theoretical Physics, Vol. 5, Pergamon Press, Oxford, 1969.
[25] W. Bazela, J. Leciejewicz, H. Ptasiewicz-Bak, A. Szytuła, J. Magn. Magn. Mater. 72 (1988) 85–87.
[26] S.G. Sankar, S.K. Malik, V.U.S. Rao, R. Obermyer, AIP Conf. Proc. 34 (1976) 236–238.
[27] H.M. Duh, I.S. Lyubutin, Y.C. Chen, H.F. Chen, C.H. Lin, J. Phys. Condens. Matter 10 (1998) 4457.